The average structure of An 62-66 labradorite

HANS-RUDOLF WENK

Department of Geology and Geophysics, University of California
Berkeley, California 94720

WERNER JOSWIG, TOKUHEI TAGAI, MASAAKI KOREKAWA

Institut für Kristallographie und Mineralogie
Universität Frankfurt a.M., Frankfurt, F.R. Germany

AND BRADLEY K. SMITH

Department of Geology and Geophysics, University of California
Berkeley, California 94720

Abstract

The paper reports results of X-ray and neutron structure refinements of four labradorites An 62–An 66 with different geological histories and different superstructures. A rapidly quenched crystal collected during the eruption of Surtsey (Iceland) is essentially disordered. Labradorite from massive lava flows of Lake County (Oregon) shows b reflections, and two metamorphic labradorites from the Central Alps display an intermediate plagioclase structure with e reflections. The average structure ($c = 7A$) of all four samples converging at R factors of 3–6% are virtually identical with well-defined Si/Al and smeared-out oxygen positions. We interpret this as evidence that the different superstructures consist of periodic stackings of similar basic units probably resembling those in $I\bar{1}$ anorthite but with different stacking orders. The main intensity contribution to superstructure reflections comes from displacements of oxygens in the superstructures, probably caused by Al–Si ordering.

Phase relations are illustrated in a hypothetical TTT diagram in which we summarize results from structure refinements, microstructural observations and changes during experimental heating. At high temperature (little undercooling below the critical temperature) ordering takes place by a nucleation and growth mechanism which produced $I\bar{1}$ domains separated by curved APB's (antiphase boundaries) (Lake County). At larger undercooling continuous ordering prevails, giving rise to periodic APB's and satellites in the diffraction pattern.

Introduction

Calcic plagioclase shows considerable structural variation which is expressed in superstructures and documented by reflections which appear in addition to the basic reflections present in X-ray diffraction patterns of albite (for a review and references see Smith, 1974). While the low and high albite structures are fairly well established (*e.g.* Harlow *et al.*, 1973; Prewitt *et al.*, 1976; Winter *et al.*, 1977), all superstructures of plagioclase, including anorthite, are still open to debate. Structural changes in plagioclase are on one hand caused by variations in chemical composition, while on the other hand they are also a function of the history of formation. In this paper we compare *average structures* derived from X-ray and neutron diffraction data of four specimens with almost the same chemical composition, An 62–An 66, but of different geological origin. We discuss structural features and relate them to microstructural characteristics as observed with X-ray and neutron film and diffractometer methods and electron microscopy, hoping to gain further information about the geometry and stability of intermediate plagioclase.

Material

We chose four specimens of labradorite: two of volcanic origin but a different cooling history and two from regionally metamorphic marbles and am-

Table 1. Chemical and physical properties of labradorites

	Surtsey	Lake County	Verzasca	Sissone
Weight percent oxides				
SiO_2	53.29	52.16	52.1	52.0
Al_2O_3	30.90	30.88	30.2	31.2
CaO	13.11	13.71	13.08	13.8
NaO	3.51	3.96	4.08	3.39
K_2O	.11	.12	.07	.03
Fe_2O_3	.36	.44	.02	.11
Formula based on 8 oxygens				
Si	2.38	2.35	2.37	2.34
Al	1.63	1.64	1.62	1.66
Ca	.63	.66	.64	.67
Na	.304	.35	.36	.30
K	.006	.007	.004	.002
Fe	.014	.017	.001	.004
Lattice parameters				
a (Å)	8.1736 (5)[2]	8.1747 (9)[2]	8.151 (3)[3]	8.152 (4)[3]
b (Å)	12.8736 (5)	12.8706 (6)	12.829 (5)	12.834 (6)
c (Å)	7.1022 (2)	7.1014 (3)	7.103 (4)	7.079 (4)
α (deg)	93.462 (6)	93.461 (5)	93.62 (3)	93.49 (2)
β (deg)	116.054 (5)	116.086 (5)	116.21 (3)	116.13 (2)
γ (deg)	90.475 (5)	90.514 (6)	89.70 (3)	90.40 (2)
Euler angles defining orientation of optical indicatrix				
Φ (deg)	51.8[4]	44.0[5]	40.5[6]	
Θ (deg)	35.2	34.5	33.0	
Ψ (deg)	-25.8	-17.5	-14.0	
$2V_\gamma$ (deg)	82.0	85.0	88.0	

[1] Measured with 8-channel ARL microprobe.
[2] Determined with Jagodzinski type Guinier camera by Dr. Kroll, Munster.
[3] Determined by automatic centering of 20 reflections on single crystal
    diffractometer.
[4] From E. Wenk et al. (1965).
[5] From E. Wenk (unpublished).
[6] From E. Wenk et al. (1975). Specimen Vz 624 from the same locality.

phibolites. All samples are chemically homogeneous on a microscopic scale. Their composition is close to An 65 (Table 1). Individual chemical formulas derived from microprobe analyses were used as constraints in the crystal structure refinements. Lattice constants and Euler angles defining the orientation of the optical indicatrix are listed in Table 1.

Since the geological history has a crucial influence on the development of the superstructures, a brief description of each specimen seems pertinent.

Surtsey. Large phenocrysts of labradorite were ejected during the submarine eruption of Surtsey, south of Iceland, in November 1963. Loose crystals up to 4 cm were collected by Dr. G. Sigvaldson in the beach sand of the newly-formed island. First the eruption was explosive, and during this phase a tuff consisting of translucent sideromelane glass (73%) and abundant olivine (7.7%, Fo 80) and labradorite crystals (7.3%, An 66), including the phenocrysts used in this study, was deposited (Steinthorsson, 1965). In May 1964 megacrysts of calcic plagioclase began to disappear. Steinthorsson interpreted their disappearance as resorption in a magma in which a more sodic plagioclase (groundmass plagioclase is An 53–56) is stable. We were unable to find much information in the geological literature about the temperature evolution of the Surtsey magma prior to

eruption. Steinthorsson (1972) concluded from the composition of coexisting titanomagnetite and hemo-ilmenite that the temperature of equilibration was 1020°C and the oxygen fugacity log $f_{O_2} = -11.5$. But since opaque minerals are relatively late crystallization products, 1020°C is a lower limit for the temperature at which the labradorite megacrysts formed. Direct temperature measurements in the extruding lava in fall 1964 with thermocouples gave values ranging from 1125 to 1180°C (Sigurgeirsson, 1965). We estimate that labradorite crystallized between 1100 and 1250°C, close to the liquidus temperature (~1350°C), and was quenched from a temperature above 1000°C within a few minutes.

The megacrysts are chemically very homogeneous with no observable zoning. Table 1 gives the results of new microprobe analyses which document deviations from stoichiometry. In H. R. Wenk and Wilde's (1973) vector representation, the analysis plots at a location typical of the substitution of Na by Ca plus vacancies, and we assume that the non-stoichiometric composition was attained during crystallization in the magma chamber. Optical properties are consistent with the high plagioclase series and an An content of 63 percent (E. Wenk *et al.*, 1965).

The preliminary X-ray experiments included a lattice-constant determination by Dr. Kroll, Münster, using a Jagodzinski-type Guinier camera (Table 1) and a photographic investigation using both focusing and non-focusing techniques. Figures 1a and b show strongly exposed X-ray and neutron 0kl Weissenberg photographs on which diffuse *e* and *c* reflections (first mentioned by H. R. Wenk, 1966) are observed together with strong and sharp *a* reflections. *e* reflections are streaked normal to $(01\bar{3})$ in 0kl photographs and have a spacing of $1/30A^{-1}$. Note the similarity of X-ray and neutron diffractograms.

Electron diffraction shows similar features (Fig. 2a, inset). The material is very homogeneous on submicroscopic scale also. Locally a low-contrast lamellar structure can be imaged with *a* reflections which documents weak structural or chemical heterogeneities (Fig. 2a).

Lake County. The second sample is from the "sunstone" north of Plush, Lake County, Oregon. Labradorite occurs as large phenocrysts in porphyritic basalt with augite, olivine, labradorite (An 60), and magnetite. Physical properties of the labradorite phenocrysts, which compose about 10% of the rock, have been extensively studied by Stewart *et al.* (1966). Optical properties are in better agreement with the low-plagioclase series (Table 1). On the

basis of lack of zoning Stewart *et al.* conclude that the phenocrysts formed in a magma chamber at depth under uniform conditions. They estimate a crystallization temperature of 1100°C. It seems that the primary crystallization may have been similar in Surtsey and Lake County labradorite, but that cooling in extensive lava flows was considerably slower in Lake County.

Single-crystal photographs show, in addition to *a* reflections, sharp *b* reflections as reported by Stewart *et al.* and diffuse *e* and *c* reflections. Diffuse *e* reflections can be distinguished from *b* reflections on the basis of intensity differences (Rainey and Wenk, 1978) and streaking. Diffuse streaks in *c* reflections are similar to those in the Surtsey specimen. With the electron microscope it is possible to image a domain structure with *b* reflections (Fig. 2b). We interpret the curved boundaries as APB's corresponding to those which have been observed in lunar anorthite.

Verzasca. This specimen is a regionally metamorphic labradorite of the same chemical composition from Gordemo, Verzasca Valley (E. Wenk *et al.*, 1975). While the crystals from Surtsey and Lake County grew in a liquid magma, the metamorphic one crystallized in the solid state in rocks of sedimentary origin during regional metamorphism which reached peak temperatures of 620–650°C at the sample locality in late Miocene. Cooling was slow and extended over many million years. The crystal analyzed is extraordinary because it constitutes the calcic portion of an andesine (An 38)–labradorite (An 63) intergrowth, documenting simultaneous crystallization of the two phases. Optical properties and lattice constants are those of low plagioclase. Single-crystal photographs display sharp *e* satellites with a satellite vector $\Delta h = 0.080(9)$, $\Delta k = 0.031(8)$, $\Delta l = -0.261(10)$, $T = 26.7(.3)$A, which is typical of calcic labradorites of medium grade (Wenk, 1979). With electron microscopy *e* reflections can be used to image regular *e* fringes and curved domain walls along which the periodic APB structure is distorted (Fig. 2c). *c* reflections are weaker and more diffuse than those of volcanic labradorites.

Sissone. A second metamorphic sample Sci 974 is from amphibolites in contact with tonalite in the high-grade metamorphic Bergell Alps (H. R. Wenk *et al.*, 1977). Wollastonite, spinel, corundum, andalusite, and sillimanite in associated rocks suggest crystallization temperatures between 700 and 900°C. In this amphibolite from the border zone of mobilization, labradorite composition is bimodal. The major phase is An 66 with local domains of An 50. X-ray
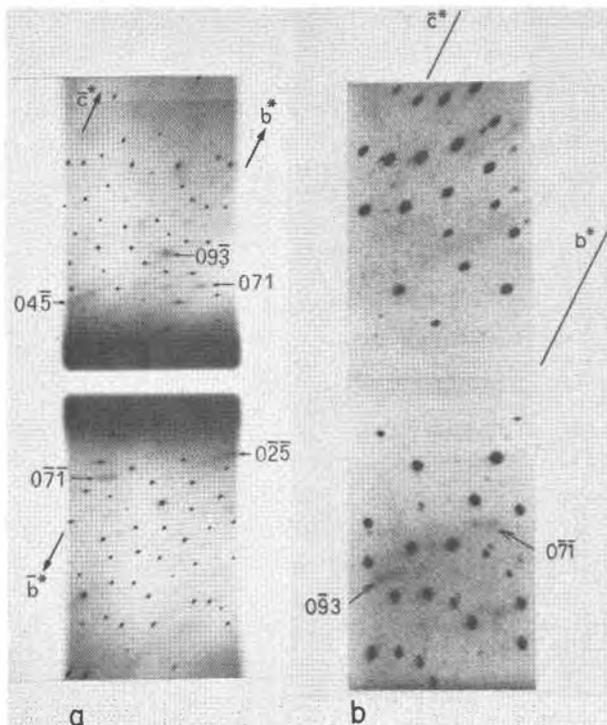

Fig. 1. b^*c^* Weissenberg photographs of Surtsey labradorite. (a) X-ray CuKα radiation using graphite monochromator (0001). φ 57.3 mm. (b) Neutron radiation λ = 1.607A, pyrolytic graphite monochromator (0001). φ 57.3 × 2 mm (Grenoble reactor).

photographs show sharp *e* reflections with a satellite vector $\Delta h = 0.015(5)$, $\Delta k = 0.080(7)$, $\Delta l = -0.109(11)$, $T = 51.4(1.1)$A, which is close to that reported for igneous plagioclase of similar composition (Gay, 1956). Electron microscopy reveals a fringe pattern which is, however, fairly irregular. *f* fringes, imaged in darkfield with *f* and *a* reflections (Fig. 2d) represent more or less periodic APB's which decompose locally by pairwise recombination into *b* boundaries (compare Wenk, 1978b). The periodic structure is best preserved in areas which contain defects, reducing the mobility of APB's.

Experimental techniques

The refinement of the average structure using only *a* reflections was done with X-ray and neutron diffraction data. (For a general appraisal of advantages and disadvantages of neutron diffraction, compare *e.g.* Will, 1969.) Neutron diffraction was used for two main reasons. Firstly, we were hoping to be able to distinguish between Al and Si, whose neutron scattering lengths show a greater difference than X-ray scattering factors (Table 2). Secondly, we anticipated getting better resolution for positional and particu-
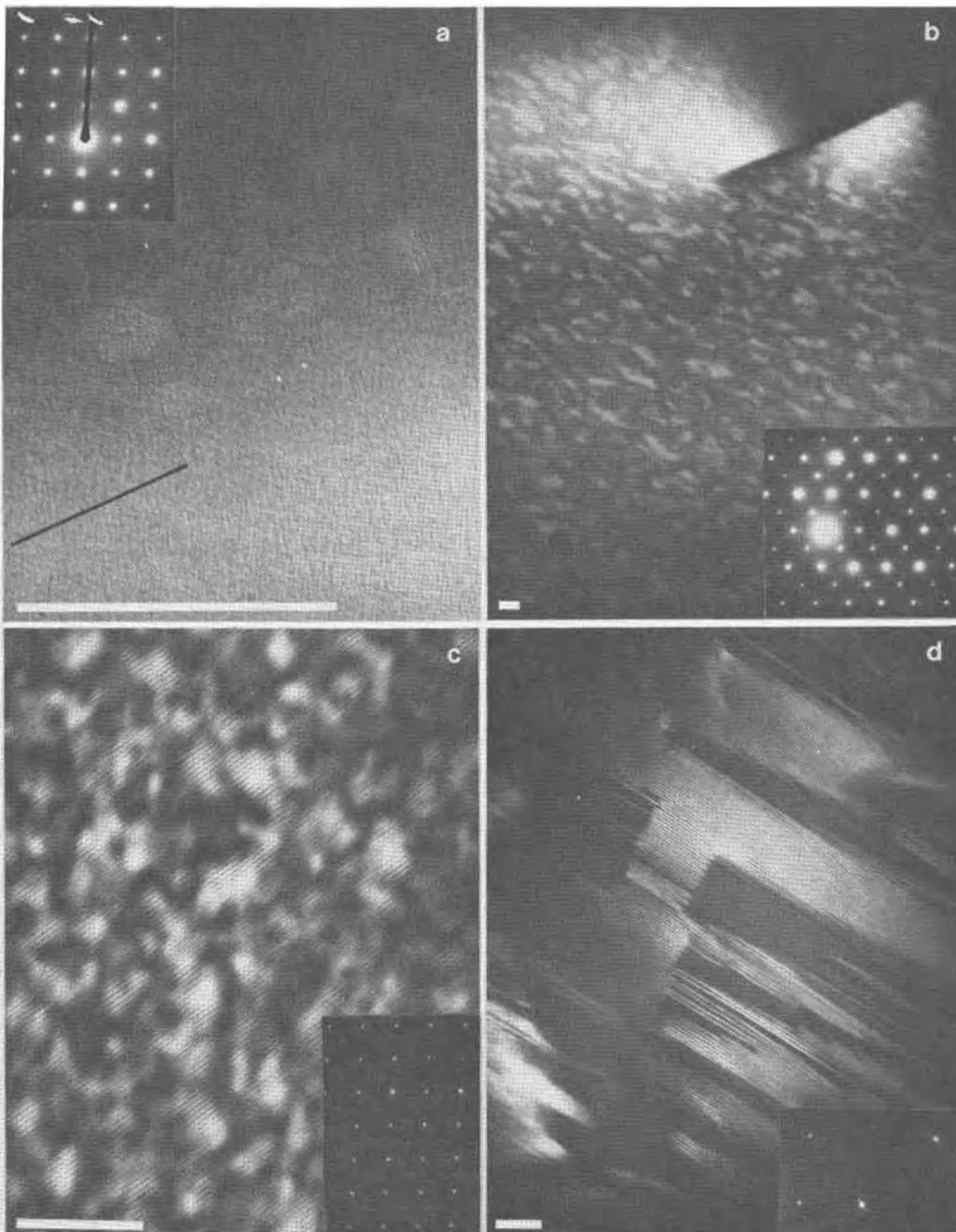
Fig. 2. Microstructural characterization of labradorites, using a JEM 100C electron microscope at 100kV accelerating voltage. Attached 0kl SAD's are taken on the same area but not in the same orientation as images. c^* is horizontal. Bars in micrographs are 1000A. (a) Surtsey. Fine structures are probably artifacts due to carbon coating and astigmatism. A possible lamellar structure is indicated by ink line. Darkfield with a reflection. (b) Lake County. Curved b APB's. Darkfield imaged with b reflection. (c) Verzasca. Periodic APB's imaged with e reflections (cf E. Wenk et al., 1975). The periodic structure is interrupted by curved boundaries. (d) Sissone. Periodic antiphase boundaries decomposing into curved b APB's imaged with a and f reflections. The diffraction pattern with e and f satellites is taken in a region with periodic APB's.

larly for thermal parameters because of the angle independence of neutron scattering lengths. Accurate thermal parameters are particularly important in average structures, where they do not only express thermal motion but also periodic or nearly periodic displacements of the atoms. Neither expectation was fulfilled. However, in the Surtsey and Lake County samples the agreements between neutron and X-ray

Table 2. Comparison of X-ray and neutron scattering factors

	X-ray (neutral - ionic)			
	$\frac{\sin\theta}{\lambda} = 0$	0.25	0.5	Neutron*
Ca	20.00 - 19.00	12.945 - 12.973	8.252 - 8.247	.490 (10)
Na	11.00 - 10.50	7.693 - 7.631	4.289 - 4.287	.351 (8)
Si	14.00 - 12.00	8.852 - 8.821	6.232 - 6.245	.415 (10)
Al	13.00 - 11.500	8.460 - 8.490	5.686 - 5.684	.345 (8)
O	8.00 - 9.00	4.805 - 4.839	2.335 - 2.314	.578 (11)

* Refined from Surtsey diffraction data. Standard deviation of least significant digits in parentheses.

refinements are excellent, which makes us confident in the significance of the derived parameters (compare Tables 4 and 5) and the reliability of both diffraction techniques.

For the X-ray investigation full data sets of intensities were collected using MoKα radiation from a graphite monochromator by the ω-scan (Surtsey) and θ–2θ scan technique (Lake County, Verzasca, and Sissone). An absorption correction ($\mu = 13.4$ cm^{-1}) was applied only to Surtsey (computer program AB-SORB of X-RAY-SYSTEM, J. M. Stewart et al., 1970).

Neutron diffraction data were collected on a four-circle diffractometer at the research reactor FR2 of the Kernforschungszentrum Karlsruhe, Germany. The approximate flux at the sample position was 6×10^5 n cm^{-2} sec^{-1}. With a neutron wavelength of $\lambda = 1.0327$A from (311) planes of a copper monochromator, intensities were measured in a ω-scan mode with variable step sizes according to the resolution curve.

For Lake County labradorite we also measured intensities of b reflections and for the Verzasca and Sissone samples pairs of e reflections, but the refinement of the superstructures is not part of this paper.

Structure refinements were done with full-matrix least-squares programs, varying 134 positional, thermal, and occupational parameters with all reflections of more than 3σ intensity. Reflections were weighted

according to individual standard deviations. Weights $w = 1/\sigma^2$ were assigned to avoid overweighting of intense reflections, where $\sigma^2 = A + \sigma_c^2 + CF_o^2$ and σ_c is the standard deviation based on counting statistics. For neutron data: $A = 20$, $C = 0.001$; for Surtsey X-ray data: $A = 3$, $C = 0.001$; for Lake County, Verzasca, and Sissone X-ray data: $A = 0$, $C = 0.0025$. Atomic scattering factors were interpolated from the table of Cromer and Mann (1968). Program CRYLSQ (from X-RAY-SYSTEM, Stewart et al., 1970) was used in Frankfurt, NUCLS6, a modified version of ORFLS (Busing et al., 1962), at Berkeley. Surtsey X-ray data were refined with both programs, and the results were identical. Refinements converged with R factors between 3 and 6% (Table 3).[1]

In the asymmetric unit of the average structure, there are 4 tetrahedral atoms, 8 oxygens, and a large cation site occupied by Ca and Na which was split into two positions of unequal occupancy. We attempted to split oxygen sites following the procedure of Toman and Frueh (1973), but the refinement did not converge. Effective electrical charges were found to be close to one-half of the full ionic charge and scattering factors were adjusted accordingly in the refinement.

Results

We notice a great similarity of most parameters in these refinements of the average structure of plagioclase (Tables 4, 5, and 6). Surtsey and Lake County labradorites are almost identical, even though the former has very diffuse and weak e satellites and the latter sharp b reflections in the diffraction pattern. Neutron and X-ray refinements of the same samples gave identical results, differences being within one standard deviation. Despite advantages of angle-in-

[1]To receive a copy of F_o and F_c tables for all crystals, order Document AM-79-118 from the Business Office, Mineralogical Society of America, 2000 Florida Avenue, N.W., Washington, D.C. 20009. Please remit $1.00 in advance for the microfiche.

Table 3. Parameters for data collection and structure refinement

	Crystal size	Diffracto meter used	Number independent reflections with |F| > 3σ	R-factor unweighted (%)	R-factor weighted (%)
Surtsey X-ray	0.27 x 0.34 x 0.2 mm	Syntex P21	2610	3.8	4.7
Surtsey neutron	2.7 x 2.0 x 2.0 mm	P32 - FR2	943	4.1	5.5
Lake County X-ray	sphere 0.2 mm	Nonius CAD 3	2306	2.7	3.9
Lake County neutron	2.0 x 2.0 x 3.0 mm	P32 - FR2	744	4.1	6.1
Verzasca X-ray	0.3 x 0.2 x 0.07 mm	Nonius CAD 3	1660	3.2	4.1
Sissone X-ray	0.2 x 0.1 x 0.04 mm	Nonius CAD 3	1672	5.0	6.5

Table 4. Atomic coordinates of labradorites. Estimated error of the least significant digits in parentheses. Refined in space group $C\bar{1}$, $c =$ 7.1A

		Surtsey X-ray		Surtsey Neutron		Lake County X-ray		Lake County Neutron		Verzasca X-ray		Sissone X-ray	
Ca-Na(1)	x	.2665	(3)	.2666	(9)	.2663	(2)	.269	(1)	.2679	(2)	.2665	(4)
	y	.9862	(5)	.987	(2)	.9834	(1)	.975	(1)	.9787	(2)	.9835	(6)
	z	.1649	(7)	.162	(3)	.1687	(2)	.176	(1)	.1659	(3)	.1692	(8)
Ca-Na(2)	x	.2723	(2)	.2733	(9)	.2709	(1)	.273	(2)	.2713	(2)	.2701	(3)
	y	.0306	(2)	.0309	(9)	.0300	(1)	.032	(1)	.0285	(1)	.0304	(2)
	z	.0952	(4)	.095	(2)	.0970	(1)	.098	(1)	.1023	(2)	.0956	(5)
$T_1(0)$	x	.00632	(10)	.0062	(3)	.00588	(5)	.0053	(6)	.00665	(7)	.00546	(14)
	y	.16304	(5)	.1632	(1)	.16271	(3)	.1632	(3)	.16503	(4)	.16279	(8)
	z	.21518	(10)	.2153	(3)	.21481	(6)	.2152	(3)	.21328	(9)	.21484	(15)
$T_1(m)$	x	.00264	(10)	.0026	(3)	.00275	(5)	.0034	(6)	.00338	(7)	.00267	(14)
	y	.81626	(5)	.8163	(1)	.81645	(3)	.8163	(4)	.81758	(4)	.81695	(8)
	z	.23099	(10)	.2306	(3)	.23109	(6)	.2314	(3)	.23205	(9)	.23107	(15)
$T_2(0)$	x	.68589	(10)	.6848	(3)	.68425	(5)	.6831	(6)	.68674	(7)	.68370	(13)
	y	.10882	(5)	.1088	(1)	.10878	(3)	.1087	(3)	.10935	(4)	.10883	(8)
	z	.31775	(11)	.3177	(3)	.31709	(6)	.3158	(3)	.31711	(9)	.31609	(15)
$T_2(m)$	x	.68100	(10)	.6806	(2)	.68086	(5)	.6796	(6)	.68204	(7)	.68035	(14)
	y	.87870	(5)	.8790	(1)	.87873	(3)	.8786	(3)	.87952	(4)	.87876	(8)
	z	.35715	(10)	.3571	(3)	.35765	(6)	.3584	(3)	.35720	(9)	.35693	(15)
$O_A(1)$	x	.0042	(3)	.0039	(2)	.0027	(2)	.0029	(4)	.0033	(2)	.0012	(4)
	y	.1290	(2)	.1290	(1)	.1281	(1)	.1279	(2)	.1303	(1)	.1274	(2)
	z	.9811	(3)	.9808	(2)	.9796	(2)	.9794	(2)	.9779	(2)	.9783	(4)
$O_A(2)$	x	.5798	(3)	.5799	(2)	.5787	(1)	.5794	(4)	.5833	(2)	.5777	(3)
	y	.9914	(1)	.9912	(1)	.9913	(1)	.9913	(2)	.9932	(1)	.9918	(2)
	z	.2789	(3)	.2786	(2)	.2777	(2)	.2784	(2)	.2788	(2)	.2765	(2)
$O_B(0)$	x	.8131	(3)	.8130	(2)	.8121	(2)	.8123	(5)	.8127	(2)	.8100	(4)
	y	.1037	(2)	.1036	(1)	.1033	(1)	.1030	(3)	.1068	(1)	.1031	(2)
	z	.1886	(4)	.1892	(3)	.1879	(2)	.1882	(3)	.1902	(2)	.1851	(4)
$O_B(m)$	x	.8156	(3)	.8158	(2)	.8152	(2)	.8160	(5)	.8170	(2)	.8140	(4)
	y	.8532	(2)	.8530	(1)	.8540	(1)	.8537	(3)	.8527	(1)	.8539	(2)
	z	.2435	(4)	.2444	(3)	.2435	(2)	.2444	(3)	.2466	(3)	.2410	(5)
$O_C(0)$	x	.0139	(3)	.0143	(2)	.0141	(2)	.0145	(4)	.0145	(2)	.0141	(4)
	y	.2895	(2)	.2895	(1)	.2892	(1)	.2869	(3)	.2931	(1)	.2893	(2)
	z	.2818	(3)	.2817	(2)	.2830	(2)	.2823	(3)	.2778	(2)	.2821	(4)
$O_C(m)$	x	.0125	(3)	.0122	(2)	.0115	(2)	.0117	(5)	.0163	(2)	.0110	(4)
	y	.6869	(2)	.6866	(1)	.6866	(1)	.6868	(3)	.6890	(1)	.6864	(2)
	z	.2133	(3)	.2130	(2)	.2118	(2)	.2126	(3)	.2174	(2)	.2108	(4)
$O_D(0)$	x	.1979	(3)	.1972	(2)	.1976	(2)	.1974	(4)	.1990	(2)	.1967	(4)
	y	.1073	(2)	.1074	(1)	.1065	(1)	.1065	(2)	.1082	(1)	.1064	(1)
	z	.3822	(3)	.3816	(3)	.3816	(2)	.3822	(3)	.3850	(2)	.3798	(4)
$O_D(m)$	x	.1900	(3)	.1902	(2)	.1906	(2)	.1905	(5)	.1889	(2)	.1903	(4)
	y	.8661	(2)	.8660	(1)	.8657	(1)	.8656	(3)	.8671	(1)	.8662	(2)
	z	.4292	(3)	.4293	(3)	.4307	(2)	.4299	(3)	.4314	(2)	.4315	(4)

dependent scattering amplitudes and lack of absorption uncertainties, standard deviations for all parameters are higher in the case of neutrons, which we attribute to the fact that a rather large crystal had to be used and the number of measured intensities was much smaller.

Atomic positions

From atomic positions selected interatomic distances and angles (Table 7) were calculated. Of these average ⟨T–O⟩ distances are most informative, be-

cause they have been used to derive the Al–Si distribution, assuming a linear relationship between bond-lengths and Al–Si occupancy (Ribbe and Gibbs, 1969; Ribbe *et al.*, 1974). In all four samples we find that $T_1(m) = T_2(m) = T_2(0)$ and $T_1(0)$ is larger, in accordance with previous determinations of sodic plagioclase (Fig. 3a). There is a larger difference in size in the metamorphic crystals, implying that Al has a site preference for $T_1(0)$, but average bond-lengths are nowhere close to those of fully-ordered structures (*e.g.* for low albite: ⟨Al–O⟩ = 1.743A, ⟨Si–

Table 5. Anisotropic thermal parameters of labradorite ($\beta\times100$). Estimated errors of the least significant digits in parentheses. Temperature factors are of the form exp $[-(\beta_{11}h^2 + \beta_{22}k^2 + \beta_{33}l^2 + 2\beta_{12}hk + 2\beta_{13}hl + 2\beta_{23}kl)]$

		Surtsey X-ray		Surtsey Neutron		Lake County X-ray		Lake County Neutron		Verzasca X-ray		Sissone X-ray	
Ca-Na (1)	β 11	.47	(3)	.61	(12)	.479	(18)	.51	(11)	.54	(3)	.43	(4)
	β 22	.95	(4)	.99	(16)	.661	(12)	.52	(20)	.764	(17)	.79	(5)
	β 33	1.56	(8)	1.80	(33)	1.01	(3)	1.87	(41)	1.53	(6)	1.13	(10)
	β 12	-.23	(2)	-.24	(7)	-.197	(11)	-.10	(8)	-.184	(16)	-.24	(3)
	β 13	.48	(4)	.58	(13)	.372	(18)	.08	(12)	.49	(3)	.45	(5)
	β 23	-.74	(5)	-.73	(20)	-.447	(15)	-.34	(14)	-.57	(2)	-.62	(6)
Ca-Na (2)	β 11	.34	(2)	.21	(10)	.434	(10)	.50	(17)	.364	(19)	.35	(3)
	β 22	.276	(10)	.31	(5)	.338	(4)	.33	(11)	.293	(9)	.267	(15)
	β 33	.87	(4)	1.02	(18)	.960	(15)	1.00	(35)	1.00	(4)	.70	(5)
	β 12	.127	(10)	.18	(4)	.115	(5)	.35	(17)	.117	(10)	.104	(14)
	β 13	.11	(2)	.12	(8)	.085	(10)	-.31	(15)	.089	(19)	.13	(3)
	β 23	-.157	(14)	-.04	(7)	-.221	(6)	-.47	(19)	-.172	(13)	-.11	(2)
$T_1(0)$	β 11	.33	(3)	.37	(5)	.431	(11)	.49	(9)	.342	(15)	.52	(3)
	β 22	.120	(8)	.18	(2)	.164	(4)	.15	(3)	.177	(5)	.249	(9)
	β 33	.42	(3)	.77	(6)	.498	(15)	.68	(11)	.44	(2)	.40	(3)
	β 12	-.043	(5)	-.00	(1)	-.043	(3)	-.04	(4)	-.048	(4)	-.039	(9)
	β 13	.153	(15)	.25	(4)	.174	(7)	-.00	(8)	.140	(10)	.190	(19)
	β 23	.022	(5)	.04	(2)	.035	(3)	.03	(5)	.046	(5)	.065	(9)
$T_1(m)$	β 11	.342	(14)	.42	(5)	.365	(7)	.48	(9)	.335	(10)	.52	(3)
	β 22	.126	(4)	.20	(2)	.139	(2)	.20	(3)	.172	(4)	.236	(9)
	β 33	.389	(17)	.75	(6)	.329	(9)	.62	(11)	.347	(16)	.35	(3)
	β 12	.090	(5)	.12	(2)	.071	(3)	.06	(4)	.121	(4)	.126	(8)
	β 13	.145	(11)	.32	(4)	.121	(6)	.03	(8)	.119	(9)	.184	(18)
	β 23	.020	(5)	.03	(2)	.003	(3)	.03	(5)	.022	(5)	.032	(9)
$T_2(0)$	β 11	.30	(3)	.34	(5)	.331	(11)	.51	(9)	.226	(14)	.24	(3)
	β 22	.091	(8)	.15	(1)	.107	(4)	1.89	(3)	.082	(5)	.123	(10)
	β 33	.62	(3)	.89	(6)	.491	(15)	.46	(11)	.40	(2)	.24	(4)
	β 12	.024	(5)	.05	(2)	.016	(3)	.02	(4)	.033	(4)	.055	(8)
	β 13	.144	(16)	.29	(4)	.120	(7)	.02	(8)	.082	(10)	.07	(2)
	β 23	.013	(5)	.02	(2)	.000	(3)	-.02	(4)	.008	(5)	-.010	(9)
$T_2(m)$	β 11	.25	(3)	.32	(5)	.331	(11)	.47	(9)	.263	(14)	.39	(3)
	β 22	.070	(9)	.13	(2)	.113	(4)	.12	(3)	.108	(5)	.191	(9)
	β 33	.49	(4)	.95	(7)	.508	(15)	.59	(12)	.46	(2)	.46	(4)
	β 12	.017	(5)	.03	(2)	.005	(3)	-.05	(4)	.019	(4)	.034	(8)
	β 13	.128	(16)	.34	(4)	.126	(7)	-.03	(8)	.141	(10)	.136	(19)
	β 23	.043	(5)	.06	(2)	.049	(3)	-.01	(4)	.051	(5)	.095	(10)

O⟩ = 1.612A, Harlow *et al.*, 1973; or for anorthite: ⟨Al–O⟩ = 1.746A and 1.756A, ⟨Si–O⟩ = 1.613 and 1.623A, Czank, 1973). This is not due to partial order but to the fact that in the average structure ($c = 7$A) of ordered anorthite Al and Si are superposed, resulting in an equal distribution of Al and Si over all four T sites (⟨T–O⟩ ~ 1.685A) (Fig. 3c). Figure 4 is a plot of ⟨T–O⟩ distances of average structures of plagioclase, which shows that the size of the tetrahedra does not vary linearly with the An content, implying a different Al–Si ordering pattern in chemically intermediate plagioclase from end members or indicating that the size–occupancy relation is not linear. In fact, the size of the Al site in sodic plagioclase seems much more sensitive to minor Si substitution than does the size of the Si site to Al substitution, which could be explained by a regular solution model with Al close to the radius-ratio limits from tetrahedral coordination being more unstable. Surt-

sey, Lake County, and Sissone follow closely the general trend, while for Verzasca the difference between $T_1(0)$ and the other three sites is slightly larger.

We tried to refine the Al/Si distribution directly, based on differences in scattering power. We are at the limit of resolution but in most refinements the $T_1(0)$ site is slightly lighter and therefore preferentially occupied by Al with fewer electrons than Si.

Thermal parameters

Anisotropic temperature factors (in Table 5 we list β_{ij}) for T atoms are surprisingly small, almost of the same magnitude as in refinements of anorthite (Wainwright and Starkey, 1969). This indicates that in the superstructures of the plagioclases we studied atomic shifts of T atoms from average positions are minimal. Oxygen atoms, on the other hand, have larger and strongly anisotropic temperature factors in contrast to *e.g.* low albite. This is illustrated in ORTEP

Table 5. (continued)

		Surtsey X-ray		Surtsey Neutron		Lake County X-ray		Lake County Neutron		Verzasca X-ray		Sissone X-ray	
$O_A(1)$	$\beta 11$	1.14	(4)	1.08	(4)	1.119	(22)	1.19	(7)	1.00	(3)	1.31	(6)
	$\beta 22$	.287	(11)	.34	(1)	.289	(6)	.29	(2)	.364	(10)	.408	(19)
	$\beta 33$	.80	(4)	1.14	(5)	.645	(23)	.60	(9)	.85	(4)	.50	(6)
	$\beta 12$	.101	(18)	.10	(1)	.087	(9)	.05	(3)	.068	(13)	.07	(3)
	$\beta 13$	.58	(4)	.71	(3)	.551	(19)	.39	(6)	.55	(3)	.56	(5)
	$\beta 23$	.086	(17)	.11	(2)	.088	(10)	.10	(3)	.132	(15)	.05	(3)
$O_A(2)$	$\beta 11$	.43	(3)	.47	(3)	.495	(16)	.49	(6)	.50	(2)	.68	(5)
	$\beta 22$	.146	(9)	.19	(1)	.158	(5)	.19	(2)	.187	(8)	.275	(16)
	$\beta 33$	.99	(4)	1.25	(4)	.789	(22)	1.04	(9)	.79	(4)	.63	(6)
	$\beta 12$	.017	(13)	.04	(1)	.010	(7)	-.01	(3)	-.003	(10)	.02	(2)
	$\beta 13$	.26	(3)	.35	(3)	.184	(15)	.17	(6)	.17	(2)	.25	(4)
	$\beta 23$	.079	(15)	.09	(1)	.060	(8)	.02	(3)	.079	(12)	.06	(2)
$O_B(0)$	$\beta 11$	.82	(4)	.80	(3)	.853	(20)	.90	(7)	.75	(3)	.89	(5)
	$\beta 22$	.192	(10)	.26	(1)	.213	(6)	.26	(2)	.233	(9)	.360	(19)
	$\beta 33$	1.47	(5)	1.72	(5)	1.321	(29)	1.45	(9)	1.20	(4)	1.43	(8)
	$\beta 12$	-.041	(16)	-.03	(1)	-.064	(8)	-.06	(3)	-.047	(11)	-.07	(3)
	$\beta 13$	.67	(4)	.76	(3)	.564	(20)	.39	(7)	.58	(3)	.58	(5)
	$\beta 23$	-.031	(17)	-.01	(2)	-.047	(10)	-.12	(4)	-.008	(14)	-.02	(3)
$O_B(m)$	$\beta 11$	.82	(4)	.80	(3)	.868	(22)	.86	(8)	.84	(3)	.87	(6)
	$\beta 22$	.269	(12)	.34	(1)	.294	(7)	.31	(3)	.309	(10)	.39	(2)
	$\beta 33$	2.12	(6)	2.36	(5)	2.168	(38)	2.68	(11)	1.91	(5)	2.34	(10)
	$\beta 12$	.081	(17)	.11	(1)	.054	(10)	.06	(3)	.070	(13)	.08	(3)
	$\beta 13$	.79	(4)	.97	(4)	.743	(24)	.59	(8)	.81	(3)	.65	(6)
	$\beta 23$	-.07	(2)	-.04	(2)	-.107	(13)	-.10	(4)	-.031	(17)	-.10	(4)
$O_C(0)$	$\beta 11$	.72	(4)	.69	(3)	.681	(7)	.71	(7)	.67	(3)	.76	(5)
	$\beta 22$	.242	(11)	.28	(1)	.280	(7)	.28	(2)	.306	(9)	.45	(2)
	$\beta 33$	1.22	(5)	1.46	(5)	1.179	(28)	1.28	(9)	1.08	(4)	1.02	(7)
	$\beta 12$	-.056	(16)	-.06	(1)	-.075	(9)	-.08	(3)	-.088	(11)	-.04	(3)
	$\beta 13$	.45	(4)	.51	(3)	.370	(18)	.20	(6)	.32	(3)	.34	(5)
	$\beta 23$	.048	(17)	.06	(2)	.080	(11)	.15	(3)	.073	(15)	.16	(3)
$O_C(m)$	$\beta 11$	.74	(4)	.69	(3)	.657	(18)	.86	(7)	.75	(3)	.84	(5)
	$\beta 22$	.244	(11)	.29	(1)	.269	(6)	.39	(3)	.325	(10)	.403	(19)
	$\beta 33$	.97	(4)	1.16	(4)	.880	(25)	1.17	(9)	.93	(4)	.70	(7)
	$\beta 12$	.181	(16)	.16	(1)	.117	(8)	.17	(3)	.238	(12)	.19	(2)
	$\beta 13$	.21	(3)	.27	(3)	.159	(17)	.22	(6)	.14	(3)	.04	(5)
	$\beta 23$	-.02	(2)	-.03	(1)	-.077	(10)	-.00	(3)	-.085	(14)	-.14	(3)
$O_D(0)$	$\beta 11$	.70	(4)	.69	(3)	.729	(18)	.74	(7)	.71	(3)	.89	(5)
	$\beta 22$	.226	(10)	.27	(1)	.231	(6)	.24	(2)	.265	(9)	.328	(19)
	$\beta 33$	.86	(4)	1.13	(4)	.754	(24)	1.00	(9)	.71	(4)	.60	(6)
	$\beta 12$	.060	(15)	.06	(1)	.027	(8)	.05	(3)	-.004	(11)	.00	(2)
	$\beta 13$	.15	(3)	.25	(3)	.058	(17)	-.13	(6)	.09	(2)	.04	(4)
	$\beta 23$	.055	(16)	.06	(1)	.043	(9)	.10	(3)	.044	(13)	.01	(3)
$O_D(m)$	$\beta 11$	.75	(4)	.72	(3)	.810	20)	.82	(7)	.75	(3)	.95	(5)
	$\beta 22$	.263	(11)	.32	(1)	.301	(7)	.31	(2)	.290	(9)	.41	(2)
	$\beta 33$	1.18	(5)	1.48	(5)	.998	(27)	1.10	(10)	.86	(4)	.90	(7)
	$\beta 12$	.085	(17)	.07	(1)	.070	(9)	.07	(3)	.044	(12)	.15	(3)
	$\beta 13$	-.01	(4)	.13	(3)	-.055	(18)	-.79	(7)	.08	(2)	-.04	(5)
	$\beta 23$	-.062	(18)	-.05	(2)	-.079	(11)	-.09	(4)	-.045	(14)	-.07	(3)

plots in Figure 3, where 98% probability contours are drawn. Assuming a real mean amplitude of thermal vibration of 0.12A (B = 1.1) for oxygen (e.g. low albite, Winter et al., 1977) then the high apparent temperature factors for O_B and O_D atoms ($B_u \sim 2.5$) has to be explained by actual atomic displacements of at least 0.1A. Thermal parameters of all four specimens are similar.

Splitting of Ca/Na

We have followed the procedure applied by Ribbe et al. (1969) to albite and by Czank (1973) to anorthite to split the Ca/Na atoms, distributing Ca/Na unequally over two positions. Positional, thermal, and occupational parameters were refined independently and the R factor improved. As Czank (1973)

showed for anorthite, splitting persists up to high temperatures but occupation of the split positions becomes more and more similar with increasing temperature. He interprets it as a statistical distribution of the large cation over two positions of different energy, with preferences determined by the environment (such as the Al/Si distribution in impure anorthite), rather than a thermal vibration between two positions (Quareni and Taylor, 1971).

Splitting of the Ca/Na site is visible in Fourier maps but only if low-order components, which include several very strong reflections, are omitted from the summation. Figure 5 shows Fourier maps with $d_{hkl} < 1.25$A for all four samples and documents a great similarity of this structural detail. We determine from Fourier maps and direct refinement of occupancies (Table 6) that the Ca/Na (2) peak is preferentially occupied over Ca/Na (1), which is in agreement with Czank's findings. The separation of split Ca/Na atoms is about 0.8A in all four structures (Table 7) and is very close to that of anorthite, indicating that this aspect of the plagioclase structure is similar over a wide composition range (e.g. Quareni and Taylor, 1971, and Winter et al., 1977, find it even in low albite; and Prewitt et al., 1976, document it in high albite), and in crystals with different thermal histories.

Extinction coefficient

At the last stages of the refinements, relatively large extinctions of strong low-angle reflections were encountered in the volcanic samples, and an isotropic correction for secondary extinction was carried out (Zachariasen, 1968). Values for extinction coefficients of Surtsey [$.156(3) \times 10^{-5}$] and Lake County [$0.80(4) \times 10^{-5}$] are rather large, indicating a high perfection of the volcanic crystals, while metamorphic crystals showed low extinction ($<10^{-7}$).

Discussion

Average structure

In this paper we will discuss average structures and atomic parameters that have been derived from main reflections only (type *a*). All information is contained in a $c = 7$A unit cell with space-group symmetry $C\bar{1}$. The presence of superstructure reflections in the diffraction pattern (*b* and *e* type) indicates that this is not the true structure. Physically the average structure is best visualized as a projection of the larger

Table 6. Occupancies of Ca–Na positions

	Refined occupancies		Electron density of Ca-Na (2) peak in e Å^{-3} (compare Figure 5)
	Ca-Na (1)	Ca-Na (2)	
Surtsey	.447 (9)	.553	38
Lake County	.366 (2)	.634	47
Verzasca	.486 (2)	.514	43
Sissone	.438 (10)	.561	41

unit cell of the true structure into the unit cell of albite. This means that corresponding atoms with slight atomic shifts in the true structure appear in the average structure as partially occupied sites, very close to each other. If they are far enough separated, their positions can be refined as split atoms such as Ca/Na in our refinement. Alternatively an average site may be calculated and displacements are integrated in an apparent temperature factor which is generally larger than that of the true structure. In order to deconvolute the average structure, one has to use the intensities of superreflections.

The superstructure of plagioclase with *b* reflections (body-centered anorthite) is well established (*e.g.* Fleet *et al.*, 1966; Czank, 1973; Berking, 1976; Tagai *et al.*, 1978). For intermediate plagioclase with *e* reflections, several more or less quantitative models have been proposed, which all differ in important respects and emphasize either Ca/Na or Al/Si order, or wavelike or discrete periodic atomic displacements (Kitamura and Morimoto, 1977; Korekawa *et al.*, 1978; Toman and Frueh, 1976). In this paper we do not discuss detailed atomic arrangements in the superstructures, but wish to see how results from average structure determinations constrain models for the true structure of labradorites.

The principal conclusion is that all four average structures are very similar, even though Verzasca and Sissone have sharp *e* satellites, Lake County has *b* reflections, and Surtsey is highly disordered. This seems to imply that all crystals are composed of similar structural units, and differences are mainly due to the stacking of these units. In intermediate plagioclase (*e* plagioclase) they are stacked in a long-range periodic pattern with antiphase relationships which are expressed in extinctions in the satellite diffraction pattern (Korekawa, 1967). In *b* plagioclase units alternate regularly along the *z* axis, causing a doubling
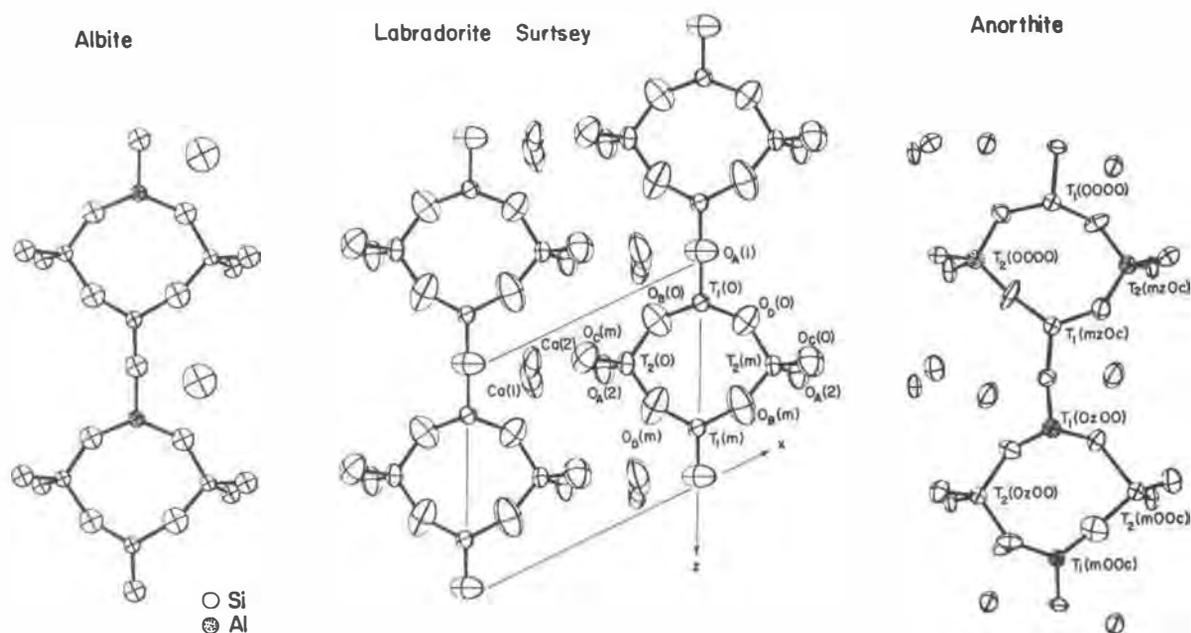
Fig. 3. Comparison of the average structure of Surtsey labradorite with the structures of low albite and anorthite. ORTEP plots with 98% probability contours of the vicinity of the xzo plane are shown. (a) Albite from Wainwright in Smith (1974, p. 86). (b) Surtsey. (c) Anorthite from Wainwright and Starkey (1971).

of c. The relative displacement between units is 1/2 [001] (which is equal to 1/2 [110] in space group $I\overline{1}$; compare Müller et al., 1973). In disordered plagioclase distribution of the units is random and neither e nor b reflections are observed. (Very weak and diffuse c and e reflections are present on strongly-exposed photographs of Surtsey, indicating that even this rapidly-quenched volcanic crystal shows at least short-range order.)

A second feature of all refinements is that temperature factors for tetrahedral sites are of the same magnitude (Fig. 3b) as those observed in albite (Fig. 3a) and anorthite (Fig. 3c). Averaging does not smear out atomic positions of Al and Si and displacements in the true structure from average atomic positions are minimal. This is different for oxygens, particularly $O_B(m)$, $O_B(0)$, $O_D(m)$, and $O_D(0)$, which have much larger and more strongly anisotropic temperature factors than equivalent atoms in the resolved albite and anorthite structures, and must therefore be due to displacements and not anisotropic thermal vibration. The oxygen displacements in the average structures are plausible by comparison with the anorthite structure (Fig. 3c, from Wainwright and Starkey, 1971), with distorted chains of tetrahedra extending parallel to x. Anisotropic temperature factors for Surtsey are identical to those of the other

samples which show a well-developed superstructure. This implies that this rapidly-quenched crystal with essentially only a reflections has not a low or high albite structure. Rather Surtsey is composed of the same structural units as the others, except that stacking is random. The sharp split of the Ca/Na position in all four samples, including e plagioclase, is evidence for stacking of units with discrete displacements rather than a sinusoidal variation (e.g. Fig. 4 in Kitamura and Morimoto, 1977).

A third striking observation is that intensities of b and e reflections are similar in X-ray and neutron diffraction photographs (Fig. 1), even though scattering powers of atoms are different (Table 2). This supports a model with atomic displacements rather than occupational differences.

Another structure with periodic stacking is ferroelectric $NaNO_2$. Böhm (1977) has used this example to extend the satellite theory of Korekawa (1967), which is mainly concerned with transverse and longitudinal displacement and density waves, to include periodic stacking, and was able to explain intensity variations with glancing angle. In general, several orders of satellites are expected at medium and high glancing angles if a modulated structure contains periodic atomic displacements. Higher orders have not been observed in $NaNO_2$, nor in intermediate plagio-

clase, where the main superstructure intensity is coming from only one pair of satellites (*e* reflections). (In some calcic labradorites and bytownites additional *f* reflections are present, satellitic about *a* positions.)

We have noted above that average structures of labradorite are very suggestive of stacking of two structural elements, both ~7A. These structural elements are similar but differ in Al/Si arrangements, displacements of oxygen atoms, and possibly occupation and position of Ca/Na. As in $NaNO_2$, A and B are both acentric and related to each other by a center of symmetry (compare Fig. 3c). A combination of these elements in $I\bar{1}$ symmetry ($c = 14A$) with A on 0,0,0 and ½,½,½ and B on 0,0,½ and ½,½,0 (Fig. 6a) produces the superstructure of body-centered plagioclase with *b* reflections (Tagai *et al.*, 1978).

For labradorite with *e* reflections the same elements may build the superstructure in a periodic antiphase pattern with less-ordered transition zones

at the domain boundaries (Fig. 6b; Korekawa *et al.*, 1978). In this model orientation and spacing of the periodic APB's are a function of the extent of ordered bands relative to disordered zones which separate them. The average structure does not allow extraction of quantitative details about the atomic distribution in the superstructures, but we may imply further information from the microstructure of the four samples, their geological history, and some additional heating experiments.

Microstructure

All four samples appear to be chemically homogeneous. Apart from minor local lamellar structures in

Fig. 4. Plot of average T–O distances of average plagioclase structures *vs.* composition. [Samples plotted include Wainwright and Starkey, 1971 (k); Berking, 1976 (j); Fleet *et al.*, 1966 (i); Klein and Korekawa, 1976 (g); Phillips *et al.*, 1971 (c, d); Prewitt *et al.*, 1976 (b); and Winter *et al.*, 1977 (a), in addition to the four new refinements and unpublished data of three metamorphic plagioclases (e, f, h).]

Table 7. Ca–Na(1)—Ca–Na(2) and T–O bond lengths (in A) and tetrahedral bond angles (in °) taken from X-ray refinements. Estimated error in parentheses

|	Surtsey		Lake County		Verzasca		Sissone	
Ca-Na(1) - Ca-Na(2)	.793	(5)	.821	(2)	.813	(7)	.828	(9)
T$_1$(O) - OA(1)	1.686	(2)	1.692	(1)	1.691	(2)	1.693	(3)
OB(O)	1.678	(2)	1.679	(1)	1.689	(2)	1.685	(3)
OC(O)	1.661	(2)	1.662	(1)	1.671	(2)	1.656	(3)
OD(O)	1.693	(2)	1.697	(1)	1.700	(2)	1.683	(3)
Average	1.680		1.683		1.688		1.679	
T$_1$(O) ATB	101.6	(1)	101.27	(6)	102.10	(9)	100.3	(2)
ATC	117.1	(1)	117.56	(6)	116.50	(8)	117.6	(1)
ATD	101.5	(1)	101.30	(6)	102.68	(9)	101.1	(1)
BTC	111.8	(1)	111.89	(6)	111.93	(8)	112.2	(1)
BTD	113.9	(1)	113.89	(6)	112.94	(8)	114.3	(2)
CTD	110.5	(1)	110.40	(6)	110.24	(8)	110.7	(1)
T$_1$(m) - OA(1)	1.680	(2)	1.680	(1)	1.652	(2)	1.672	(3)
OB(m)	1.642	(3)	1.649	(1)	1.627	(2)	1.642	(3)
OC(m)	1.668	(2)	1.673	(1)	1.652	(2)	1.677	(3)
OD(m)	1.649	(2)	1.652	(1)	1.643	(2)	1.649	(3)
Average	1.660		1.664		1.644		1.660	
T$_1$(m) ATB	104.1	(1)	104.12	(7)	105.89	(9)	104.2	(2)
ATC	112.8	(1)	112.88	(6)	112.33	(9)	112.9	(1)
ATD	105.0	(1)	104.87	(6)	105.69	(9)	104.6	(2)
BTC	111.9	(1)	112.03	(6)	110.96	(9)	111.6	(2)
BTD	113.2	(1)	113.12	(6)	112.65	(9)	113.5	(2)
CTD	109.6	(1)	109.55	(6)	109.22	(8)	109.8	(2)
T$_2$(O) - OA(2)	1.679	(2)	1.680	(1)	1.663	(1)	1.673	(3)
OB(O)	1.668	(2)	1.666	(1)	1.637	(2)	1.661	(3)
OC(m)	1.656	(2)	1.656	(1)	1.638	(2)	1.648	(3)
OD(m)	1.640	(2)	1.635	(1)	1.626	(2)	1.631	(3)
Average	1.661		1.660		1.642		1.653	
T$_2$(O) ATB	107.4	(1)	107.24	(5)	108.81	(8)	107.2	(1)
ATC	102.8	(1)	102.61	(6)	103.42	(8)	102.3	(1)
ATD	108.6	(1)	108.89	(6)	108.07	(8)	108.9	(1)
BTC	112.3	(1)	112.24	(6)	111.68	(8)	112.0	(2)
BTD	111.2	(1)	111.18	(7)	111.21	(9)	111.4	(2)
CTD	114.0	(1)	114.07	(6)	113.21	(8)	114.4	(1)
T$_2$(m) - OA(2)	1.697	(2)	1.680	(1)	1.667	(2)	1.681	(3)
OB(m)	1.650	(3)	1.650	(1)	1.634	(2)	1.650	(3)
OC(O)	1.652	(2)	1.652	(1)	1.634	(2)	1.645	(3)
OD(O)	1.669	(2)	1.670	(1)	1.648	(2)	1.680	(3)
Average	1.662		1.663		1.646		1.664	
T$_2$(m) ATB	109.4	(1)	108.91	(7)	109.05	(8)	108.7	(1)
ATC	105.7	(1)	105.66	(6)	105.61	(8)	105.8	(1)
ATD	107.4	(1)	107.52	(5)	107.73	(8)	107.6	(1)
BTC	111.1	(1)	111.29	(7)	110.81	(9)	111.0	(2)
BTD	110.4	(1)	110.49	(7)	110.26	(9)	110.8	(2)
CTD	112.6	(1)	112.73	(6)	113.16	(9)	112.8	(1)
T1-OA(1)-T1	140.1	(1)	139.63	(10)	140.89	(10)	139.2	(2)
T2-OA(2)-T2	126.3	(1)	125.95	(9)	127.17	(6)	125.8	(2)
T1-OB(O)-T2	136.2	(1)	135.98	(10)	137.92	(7)	135.2	(2)
T1-OB(m)-T2	156.1	(2)	155.81	(10)	157.40	(10)	155.0	(2)
T1-OC(O)-T2	131.1	(1)	131.36	(10)	131.15	(8)	131.6	(2)
T1-OC(m)-T2	131.6	(1)	131.13	(10)	132.94	(7)	130.9	(2)
T1-OD(O)-T2	133.2	(1)	131.86	(10)	133.24	(7)	131.6	(2)
T1-OD(m)-T2	150.6	(2)	151.06	(10)	150.85	(10)	151.3	(2)
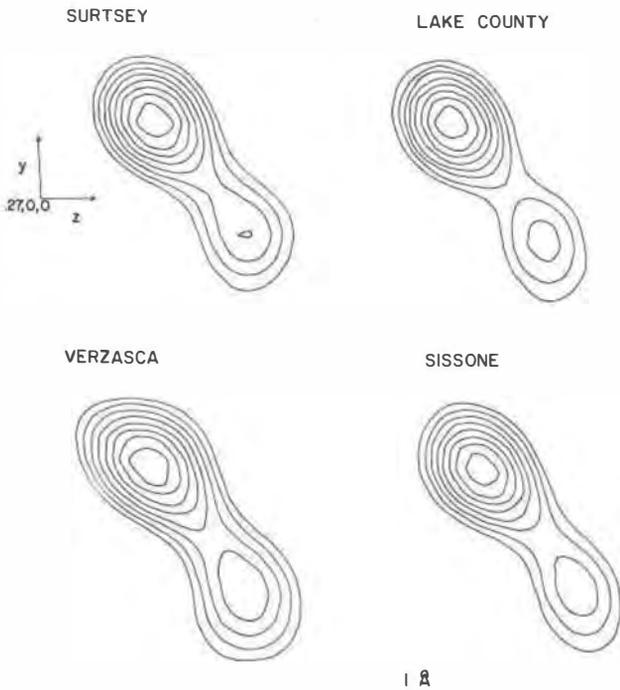
Fig. 5. Four F(obs) maps of the Ca–Na peak. Reflections with d > 1.25A are omitted from the summation to increase resolution. yz section at x = 0.27. (Compare Table 6).

Surtsey (Fig. 2) and Verzasca (E. Wenk et al., 1975, their Fig. 6c), there is no evidence for *chemical heterogeneity*. The a reflections in X-ray diffraction patterns obtained with focusing Laue technique are sharp and not split. This is in contrast to "schiller"
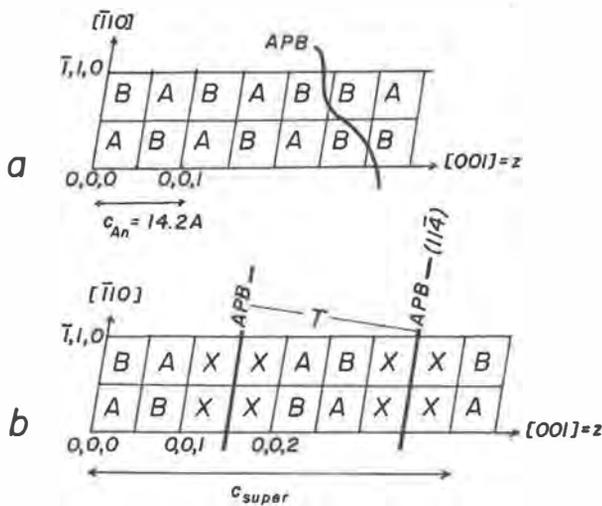
labradorites An 50–60 and bytownites An 70–85 which show chemical exsolution (*e.g.* Cliff *et al.*, 1976). There are *structural homogeneities*, though: we described antiphase domains in Lake County samples which probably formed during cooling. There are similar boundaries in the Verzasca crystal (Fig. 2e). The presence of two structures in the Lake County sample is documented by a diffraction pattern with sharp b and diffuse e reflections (Rainey and Wenk, 1978, their Fig. 4b).

In solid solutions either exsolution or ordering will occur, depending on whether repulsive or attractive forces dominate between unlike atoms. In plagioclase with two coupled substitutions both processes take place, but the four labradorite samples described here appear to be chemically homogeneous representatives from the region between the Bøggild and Huttenlocher exsolution gaps in the phase diagram (compare *e.g.* Fig. 3 in Wenk, 1979).

Ordering can take place by different mechanisms. It may start at nuclei and proceed by growth of ordered domains. Microstructures which are the result of such a mechanism are often characterized by curved APB's like those observed in Lake County crystals (Fig. 2b). Alternatively, at larger undercooling below the critical ordering temperature, or-

Fig. 6. Schematic models for the superstructure of labradorites as different stackings of units A and B. (a) Body-centered plagioclase (Tagai *et al.*, 1978). (b) Intermediate plagioclase An~50 (Korekawa *et al.*, 1978).
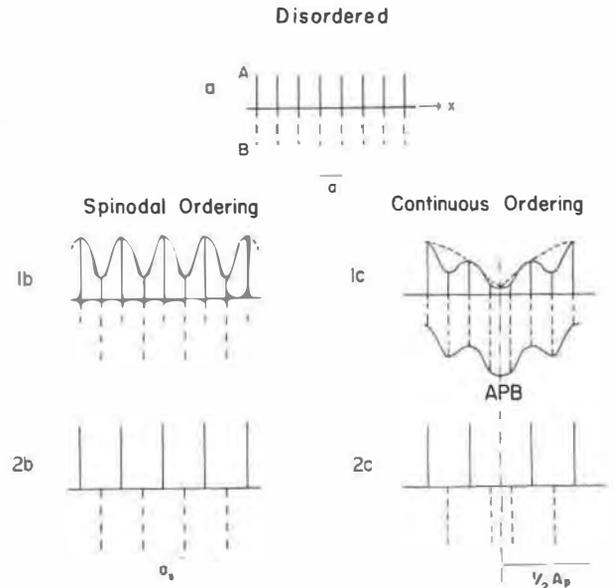
Fig. 7. Schematic diagram illustrating homogeneous ordering of two atomic species A and B in a one-dimensional crystal by a spinodal mechanism (b) with formation of a superstructure with a_s and continuous order (c) resulting in periodic APB's. Horizontal axis x is a crystal coordinate. Vertical axes give amounts of A (solid) and B (dashed) in each site.

dering may take place homogeneously throughout the crystal.

De Fontaine (1975) distinguishes between two modes of homogeneous ordering which are illustrated schematically in Figure 7. In *spinodal ordering* the new site distribution in the superstructure is attained gradually as the transformation proceeds. Ordering generally results in a superstructure with a decrease in symmetry—such as in Figure 7—or a doubling of the unit cell. In *continuous ordering* a large wavelength compositional modulation is convoluted with the short wavelength of ordering. This latter mechanism produces modulated structures with periodic APB's.

The thermal history of samples and accompanying structural changes can be traced in a time–temperature–transformation diagram (TTT) which has been used to illustrate chemical decompositions of geological samples (*e.g.* Champness and Lorimer, 1976). The analogy to ordering is not strictly applicable. Structures in the regions labeled "nucleation and growth" and "continuous ordering" could be different. Volcanic samples with *b* reflections may only have a short-range ordered Al/Si distribution adjusting for non-stoichiometry in a random pattern.

The very schematic and empirical diagram in Figure 8 shows fields for heterogeneous (or possibly homogeneous) nucleation of an ordered equilibrium structure ($I\bar{1}$ structure with *b* reflections) and for continuous ordering at conditions of undercooling (intermediate plagioclase with *e* reflections). Beginning and end of the ordering reaction are indicated. In the case of nucleation and growth the end product is a pattern of ordered domains separated by APB's. In continuous ordering a modulated structure forms which decomposes during prolonged annealing by pairwise recombination of APB's. Changes in microstructure and particularly the high mobility of ½[001]APB's are further elaborated by Wenk and Nakajima (1979), who document a whole range of transitions between *e* and *b* plagioclase simply due to different arrangements of APB's. Temperatures in Figure 8 are rough estimates, and the time coordinate is based on empirical observations.

Surtsey labradorite (Su) was rapidly quenched from temperatures close to the solidus. The cooling path barely passes through the "continuous" nose and leaves it again before ordering in a periodic pattern is complete. Lake County (LC) cooled more slowly, allowing nucleation of ordered $I\bar{1}$ domains. A small volume fraction is still disordered when the curve passes through the field of continous ordering,
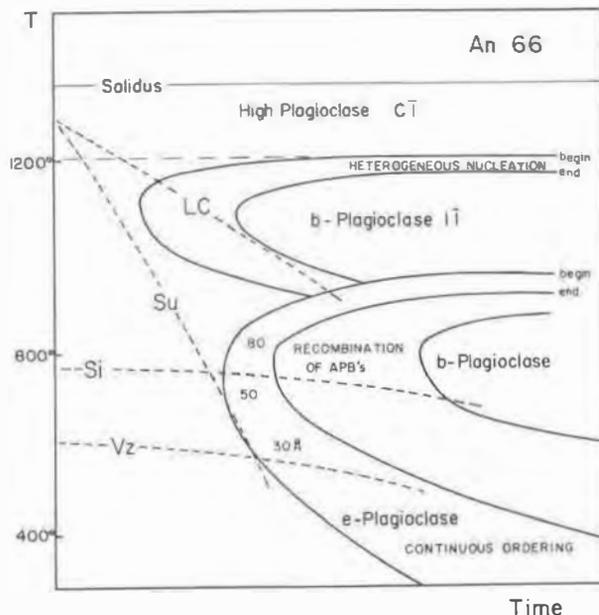

Fig. 8. Empirical TTT (time–temperature–transformation) diagram illustrating cooling histories and microstructural changes in various An 66 labradorites.

giving rise to additional weak *e* reflections. The two metamorphic samples Verzasca (Vz) and Sissone (Si) crystallized at low temperature and cooled very slowly, forming fully-ordered periodic structures. Sissone, the higher-grade plagioclase, attains a larger wavelength (51A) than Verzasca (27A) and decomposes partially by recombination of *e* APB's to *b* plagioclase.

We have done heating experiments which seem to conform with such a model (see also Tagai *et al.*, 1977). Heating Lake County crystals in a furnace at 1180°C for 1 week erases *b* reflections and *b* APB's (Fig. 9b). Our model leaves two alternatives. Either heating produces true disordering of Si and Al on tetrahedral sites or it merely causes a random stacking of still-ordered units. We prefer the latter explanation unless crystals are heated very close to the melting point. Such a mechanism requires only mobility of antiphase boundaries rather than structural rearrangements, which is in better agreement with observed changes during cooling. Consecutive slow cooling to 900°C at 25°C per day produced *b* reflections again, and darkfield images show a microstructure with small ordered domains (Fig. 9c). All these experiments were in the field of $I\bar{1}$ structures. Hydrothermal annealing of Surtsey at 870°C produces sharp *e* satellites (Wenk, 1978a), while after longer annealing at 900°C *e* reflections are replaced
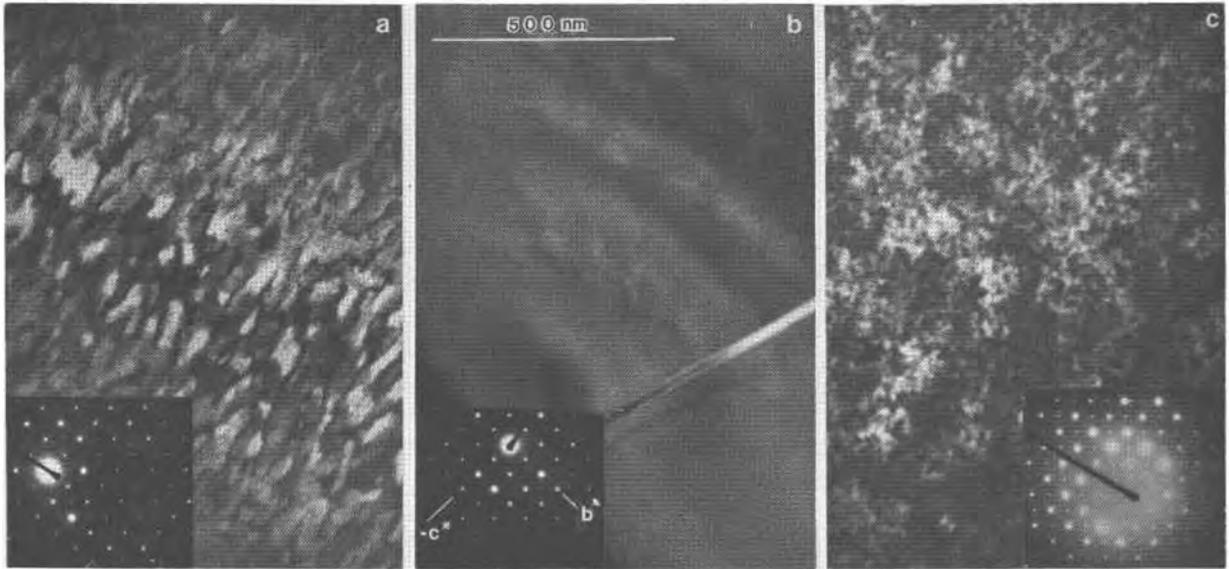
Fig. 9. Changes in microstructure of Lake County labradorite after heating (compare also Tagai *et al.*, 1977). Darkfield photographs taken with *b* reflections (a) APB's in untreated crystals. (b) APB's disappear and *b* reflections become extremely weak and diffuse after heating at 1200°C for 1 week. (c) Upon slow cooling to 900°C at 25°C per day *b* reflections appear again and small ordered domains become visible.

by *b* reflections (McConnell, 1974). The upper boundary of the field for continuous ordering is estimated to be around 900–950°C. The geological history of a sample which established the state of order has a decisive influence on changes during heat treatment, and results presented here cannot be generalized and applied to other labradorites.

c reflections

A last point to mention is the presence of diffuse *c* reflections in volcanic labradorite. Streaking is most pronounced parallel to *b**, but more exactly intensity is distributed in a disk normal to [001]. [001] is the important direction in the plagioclase structure, along which chains of 4-fold tetrahedral rings extend. In anorthite this is the direction of antiphase Al–Si stacking. We interpret these streaks as due to faults with a displacement vector ½[111] and a fault plane (010) but a poor periodicity. It is interesting that *c* reflections are weaker in metamorphic than in volcanic labradorite.

The ideas presented here, which attempt to synthesize evidence from both structural and physical features of labradorite plagioclase, are speculative and need to be corroborated further by experimental investigations of stability relations and also comparative refinements of both average and superstructures of heat-treated crystals. We hope that we can provoke other feldspar researchers to participate in this fascinating endeavor.

References

Berking, B. (1976) Die Verfeinerung der Kristallstruktur eines lunaren Plagioklases An 90. *Z. Kristallogr.*, *144*, 189–197.

Böhm, H. (1977) *Eine erweiterte Theorie der Satellitenreflexe und die Bestimmung der modulierten Struktur des Natriumnitrits.* Habilitationsschrift der Universität Münster, Münster, Germany.

Busing, W. R., K. O. Martin and H. A. Levy (1962) A FORTRAN crystallographic function and error program. *U. S. Nat. Tech. Inform. Serv. ORNL-TM-308.*

Champness, P. E. and G. W. Lorimer (1976) Exsolution in silicates. In H. R. Wenk *et al.*, Eds., *Electron Microscopy in Mineralogy*, p. 174–204. Springer, Heidelberg.

Cliff, G., P. E. Champness, H. U. Nissen and G. W. Lorimer (1976) Analytical electron microscopy of exsolution lamellae in plagioclase feldspars. In H. R. Wenk *et al.*, Eds., *Electron Microscopy in Mineralogy*, p. 258–265. Springer, Heidelberg.

Cromer, D. T. and J. Mann (1968) X-ray scattering factors computed from numerical Hartree–Fock wave functions. *Acta Crystallogr., A24*, 321–324.

Czank, M. (1973) *Strukturuntersuchungen von Anorthit im Temperaturbereich von 20°C bis 1430°C*. Ph. D. Thesis, ETH, Zürich.

de Fontaine, D. (1975) K-space symmetry rules for order–disorder reactions. *Acta Metallurgica, 23*, 553–571.

Fleet, S. G., S. Chandrasekhar and H. D. Megaw (1966) The structure of bytownite ('body-centered anorthite'). *Acta Crystallogr., 21*, 782–801.

Gay, P. (1956) The structures of the plagioclase felspars: VI. Natural intermediate plagioclases. *Mineral. Mag., 31*, 21–40.

Harlow, G. E., G. E. Brown and W. C. Hamilton (1973) Neutron diffraction study of Amelia low albite (abstr.) *Trans. Am. Geophys. Union, 54*, 497.

Kitamura, M. and N. Morimoto (1977) The superstructure of intermediate plagioclase feldspars. *Phys. Chem. Minerals, 1*, 199–212.

Klein, S. and M. Korekawa (1976) Gemittelte Struktur des Labradorits An 52. *Neues Jahrb. Mineral. Monatsh.*, 66–69.

Korekawa, M. (1967) *Theorie der Satellitenreflexe*. Habilitationsschrift der Ludwigs-Maximilians Universität, München.

———, W. Horst and T. Tagai (1978) Superstructure of labradorite An₋₅₀. *Phys. Chem. Minerals, 3*, 74–75.

McConnell, J. D. C. (1974) Analysis of the time–temperature transformation behavior of the plagioclase feldspars. In W. S. MacKenzie and J. Zussman, Eds., *The Feldspars*, p. 460–477. Manchester University Press, Manchester.

Müller, W. F., H. R. Wenk, W. L. Bell and G. Thomas (1973) Analysis of the displacement vectors of antiphase domain boundaries in anorthites ($CaAl_2Si_2O_8$). *Contrib. Mineral. Petrol., 40*, 63–74.

Phillips, M. W., A. A. Colville and P. H. Ribbe (1971) The crystal structures of two oligoclases. A comparison with low and high albite. *Z. Kristallogr., 133*, 43–65.

Prewitt, C. T., S. Sueno and J. J. Papike (1976) The crystal structure of high albite and monalbite at high temperatures. *Am. Mineral., 61*, 1213–1225.

Quareni, S. and W. H. Taylor (1971) Anisotropy of the sodium atom in low albite. *Acta Crystallogr., B27*, 281–285.

———, H. D. Megaw and W. H. Taylor (1969) The albite structures. *Acta Crystallogr., B25*, 1503–1518.

Rainey, C. S. and H. R. Wenk (1978) Intensity differences of subsidiary reflections in calcic plagioclases. *Am. Mineral., 63*, 124–131.

Ribbe, P. H. and G. V. Gibbs (1969) Statistical analysis and discussion of mean Al/Si–O bond distances and the aluminum content of tetrahedra in feldspars. *Am. Mineral., 54*, 85–94.

———, M. W. Phillips and G. V. Gibbs (1974) Tetrahedral bond length variations in feldspars. In W. S. MacKenzie and J. Zussman, Eds., *The Feldspars*, p. 25–48. Manchester University Press, Manchester.

Sigurgeirsson, T. (1965) Some geophysical measurements and observations in Surtsey 1963–1964. *Surtsey Res. Progr. Rept., 1*, 63–70.

Smith, J. V. (1974) *Feldspar Minerals. Vol. 1, Crystal Structure and Physical Properties*. Springer, New York.

Steinthorsson, S. (1965) Surtsey: petrology and chemistry. *Surtsey Res. Progr. Rept., 1*, 41–50.

——— (1972) The opaque mineralogy of Surtsey. *Surtsey Res. Progr. Rept., 6*, 152–157.

Stewart, D. B., G. W. Walker, T. L. Wright and J. J. Fahey (1966) Physical properties of calcic labradorite from Lake County, Oregon. *Am. Mineral., 51*, 177–197.

Stewart, J. M., G. J. Kruger, H. L. Ammon, C. Dickinson and S. R. Hall (1970) *The "X-RAY SYSTEM" of crystallographic programs*. Computer Science Center, University of Maryland.

Tagai, T., W. Joswig, M. Korekawa and H. R. Wenk (1977) Kristallographische Untersuchung über Huttenlocher Entmischung in Plagioklas. Collected Abstracts: *Verh. d. deutschen Physik. Ges. 1/1977*, 183.

———, ———, ——— and ——— (1978) Determination of Al/Si-distribution in a plagioclase An₆₆ using neutron diffraction data. Abstract: 11th Congress, IUCp., Warsaw.

Toman, K. and A. J. Frueh (1973) On the centrosymmetry of intermediate plagioclases. *Z. Kristallogr., 138*, 337–342.

——— and ——— (1976) Modulated structure of an intermediate plagioclase. I. Model and computation. II. Numerical results and discussion. *Acta Crystallogr., B32*, 521–525, 526–538.

Wainwright, J. E. and J. Starkey (1971) A refinement of the structure of anorthite. *Z. Kristallogr., 133*, 75–84.

Wenk, E., H. Schwander and H. R. Wenk (1965) Labradorit von Surtsey. *Acta Naturalia Islandica 2-5*. Museum, Reykjavik.

———, A. Glauser and H. Schwander (1975) Intergrowth of andesine and labradorite in marbles of the Central Alps. *Contrib. Mineral. Petrol., 53*, 311–326.

Wenk, H. R. (1966) Labradorite from Surtsey (Iceland). *Schweiz. Mineral. Petrog. Mitt., 46*, 81–84.

——— (1978a) Ordering of the intermediate plagioclase structure during heating. *Am. Mineral., 63*, 132–135.

——— (1978b) The electron microscope in earth sciences. In J. M. Sturgess, Ed., *Electron Microscopy, 1978*, vol. 3, p. 404–419. Proc. 9 Int. Congr. on Electron Microscopy, Toronto.

——— (1979) Superstructure variation in metamorphic intermediate plagioclase. *Am. Mineral., 64*, 71–76.

——— and Y. Nakajima (1979) Periodic superstructures in calcic plagioclase. *Modulated Structures 1979*, Proc. Am. Inst. Phys., 53, 317–320.

——— and W. R. Wilde (1973) Chemical anomalies of lunar plagioclase, described by substitution vectors and their relation to optical and structural properties. *Contrib. Mineral. Petrol., 41*, 89–104.

———, J. Hsiao, G. Flowers, M. Weibel, M. Ayranci and Z. Fejer (1977) A geochemical survey of granitic rocks in the Bergell Alps. *Schweiz. Mineral. Petrog. Mitt., 57*, 233–265.

Will, G. (1969) Crystal structure analysis by neutron diffraction I. *Angew. chem., 8*, 356–369.

Winter, J. K., S. Ghose and F. P. Okamura (1977) A high-temperature study of the thermal expansion and the anisotropy of the sodium atom in low albite. *Am. Mineral., 62*, 921–931.

Zachariasen, W. H. (1968) Experimental tests of the general formula for the integrated intensity of real crystals. *Acta Crystallogr., A24*, 212–216.